Microchimica Acta (2022) 189: 300
https://doi.org/10.1007/s00604-022-05383-6

ORIGINAL PAPER

Highly stable acetylcholinesterase electrochemical biosensor based on polymerized ionic liquids microgel for pesticides detection

Yu Wan[1] · Huiting Wang[1] · Ling Zhang[2] · Yaxian Chen[1] · Shun Li[1] · Jie Zhou[1] · Qian Zhang[1] · Lixin Xia[3]

Received: 22 January 2022 / Accepted: 18 June 2022 / Published online: 29 July 2022

Abstract

A highly stable electrochemical biosensor for pesticide detection was developed. For the first time polymeric ionic liquids (PILs) were introduced to construct an acetylcholinesterase (AChE) biosensor . AChE was entrapped in PILs microspheres through an emulsion polymerization reaction, where negatively charged Au nanoparticles (Au NPs) can be immobilized by the positively charged PILs, leading to improved catalytic performance. The results suggest that the positively charged PILs not only provide a biocompatible microenvironment around the enzyme molecule, stabilizing its biological activity and preventing its leakage, but also act as a modifiable interface allowing other components with electron transport properties to be loaded onto the polymer substrate, thus providing an efficient electron transport channel for the entrapped enzyme. More notably, when AChE was immobilized in a positively charged environment, the active site is closer to the electrode, promoting faster electron transfer. The detection limits of the constructed electrochemical biosensor AChE@PILs@Au NPs/GCE toward carbaryl and dichlorvos (DDVP) were 5.0×10^{-2} ng ml^{-1} and 3.9×10^{-2} ng ml^{-1}, in a wide linear range of 6.3×10^{-2}–8.8×10^{2} ng ml^{-1} and 1.3×10^{-1}–1.4×10^{3} ng ml^{-1}, respectively. More importantly, the biosensor has high thermal and storage stability, which facilitates rapid field analysis of fruits and vegetables in a variety of climates. In addition, the biosensor reported has good repeatability and selectivity and has high accuracy in the analysis of peaches, tap water, and other types of samples.

Keywords Entrapped AChE · Polymeric ionic liquids · Amperometry · Pesticides · Thermal and storage stability

Introduction

Pesticides are widely used as herbicides, insecticides, and fungicides in agriculture, industry, medicine, and other fields. However, due to their high toxicity, they pose a great threat to humans and animals [1, 2]. Conventional detection methods for pesticides include gas and liquid chromatography (GLC), high-performance liquid chromatography (HPLC), and surface-enhanced Raman spectroscopy (SERS). Although these methods have high sensitivity and low detection limits, they suffer from the disadvantages of complicated, laborious, costly instruments, and high skilled manpower [3, 4]. It is important to establish a fast and in situ method for pesticide and its derivatives analysis [5–7]. The amperometric acetylcholinesterase (AChE) biosensor has been proven to be a reasonable solution due to its advantages of simple and rapid use [3, 8]. In order to construct a high-performance biosensor, the key consideration is to select an appropriate immobilization method and supporting matrix, thereby maintaining the biological activity of AChE and accelerating electron transfer.

For the enzyme immobilization, physical adsorption, beside entrapment method, covalent bond method, chemical cross-linking method, and electrochemical polymerization, the entrapment method is of great interest because of its great potential to maintain the stability of the biosensor [9]. Polymers can create a biocompatible microenvironment for the entrapped enzyme to maintain its activity, which is conducive to improving the stability of constructed biosensors.

✉ Qian Zhang
zhangq@lnu.edu.cn; lixinxia@lnu.edu.cn

✉ Lixin Xia
zhangq@lnu.edu.cn; lixinxia@lnu.edu.cn

[1] College of Chemistry, Liaoning University, Shenyang 110036, China

[2] College of Chemistry and Chemical Engineering, Shenyang Normal University, Shenyang 110034, China

[3] Yingkou Institute of Technology, Yingkou 115014, China

More importantly, using positively charged polymers to entrap negatively charged enzymes, the performance of the constructed biosensors can be further improved. The reason is that positively charged polymers have a specific interaction with negatively charged enzymes, which results in a tighter bond for improving stability. At the same time, such a positively charged polymer can also provide a suitable microenvironment for the entrapped negatively charged AChE to achieve a favorable orientation, thus facilitating the catalytic reaction toward acetylcholine chloride (ATCl) [6, 10]. However, it is a pity that the biocompatible polymer will greatly hinder the efficient electron transfer between the entrapped AChE and the surface of the electrode due to its non-conductivity, resulting in weak electrochemical performance of the biosensor. In consequence, it is desirable to compensate for this disadvantage by the modification of high conductivity materials [11–13].

Polymeric ionic liquids (PILs) have been widely used in the field of biosensing and enzyme immobilization as their certain electronic transmission properties [9]. In terms of enzyme immobilization, Ruiz et al. reported that polymeric ionic liquid particles (PIL-MP) have been found to provide a good microenvironment for the immobilized enzyme. Based on such a type of immobilization, the sensor prepared shows excellent stability [9, 10]. Besides, PILs are also used in the assembly of nanocomposites. Assembly between different components has been achieved by polymerizing ionic liquids as inter-link, confirming the versatility of PILs [14]. Therefore, if PILs are used as a polymer matrix to entrap AChE, the following benefits will be achieved: Firstly, as a positively charged water-soluble polymer, PILs will interact strongly with AChE electrostatically, and this interaction will further enhance enzyme activity in a hydrophilic environment. Secondly, PILs can also act as a modifiable interface allowing other components with electron transport properties to be loaded on the polymer substrate, thus providing an effective electron transport channel for the entrapped enzyme. In other words, PILs could provide a good microenvironment and a potential electron transport channel for AChE to achieve the analysis of pesticides with great performance.

Herein, PILs were introduced to design and synthesize a sandwich-like core–shell structural AChE@PILs@Au NPs composite. In such a structure, PILs act as both enzyme immobilizer and modifier for the first time to construct amperometric AChE electrochemical biosensors. AChE was entrapped in the PILs to act as the inner core, while the middle layer was PILs and assembled Au NPs was the outer layer. Due to the charge property of PILs and the electron transport channel of Au NPs, the constructed electrochemical detection platform AChE@PILs@Au NPs/GCE showed a high sensitivity for the detection of carbaryl and dichlorvos (DDVP). In addition, AChE@PILs@Au NPs/GCE also exhibits high stability, including long-term stability and thermal stability.

Experimental methods

Materials and chemicals

AChE (C3389, 500 U mg^{-1} from electric eel) and ATCl were obtained from Sigma. 1-vinylimidazole, bromoethane, methanol, ethyl acetate, acetone, Span 80, hydrochloric acid, sodium dihydrogen phosphate (NaH_2PO_4), and disodium hydrogen phosphate (Na_2HPO_4) were purchased from Sinopharm Chemical Reagent Co., Ltd. N, N' methylenebisacrylamide (bis) and dodecane were purchased from Aladdin Industry (Shanghai) Co., Ltd. Ammonium persulfate (APS), N, N, N', N' Tetramethylethylenediamine (TEMED) and Tris (hydroxymethyl) methyl aminomethane (Tris) were purchased from Macklin Reagent Co., Ltd. Prepare Tris–HCl by mixing 20 mM HCl and 20 mM Tris solution. Mix the stock solutions of 0.1 M NaH_2PO_4 and 0.1 M Na_2HPO_4 to prepare a phosphate buffer. All other reagents are of analytical grade, and deionized water is used throughout the experiment.

Apparatus and measurement

All electrochemical analyses were performed through a three-electrode potentiostat/current state workstation. The amperometric sensing method was selected to obtain excellent analytical performance [4, 8]. A modified glassy carbon electrode (GCE) was used as a working electrode, the platinum electrode was used as an auxiliary electrode, and Ag/AgCl electrode was used as a reference electrode. The surface morphology of the ionic liquid-related materials was analyzed by a scanning electron microscope (scanning electron microscope, SEM, JEOL JSM-7400F) operating at 5 kV, and the tested samples were freeze-dried and prepared. Zeta sizer Nano-ZS particle analyzer (Malvern Corp, UK) was used to collect particle size distribution and Zeta potential data of various materials related to PILs. On the Perkin-Elmer instrument, the Fourier transform infrared spectrum of the sample was measured with a potassium bromide tablet as the medium. In ESCALAB 250, X-ray photoelectron spectroscopy (XPS) measurement was performed on the instrument (150 W, spot size of 500 μm, Al Kα radiation of 1486.6 eV) to obtain surface element information of various materials.

Preparation of poly ($ViEtIm^+Br^-$) (PILs) microgel with entrapped AChE (AChE@PILs).

The poly ($ViEtIm^+Br^-$) was prepared by the method of concentrated emulsion polymerization in the literature [10].

The dispersed water phase is composed of the monomer ViEtIm^{+}Br^{-} (0.125 g), AChE (50–150 U), cross-linking agent bis (0.005–0.01 g), and initiator APS (0.0025 g), in which the dispersant was 20 mM Tris–HCl. The oil phase consists of dodecane (75 μL) and spans 80 (25 μL). The emulsion was prepared by adding the dispersed water phase dropwise to the oil phase; the polymerization was started by adding TEMED to the emulsion; after a period of reaction, the precipitated polymer was washed with acetone and phosphate buffer, separated by centrifugation (4000 rpm, 10 min), and then freeze-dried.

Preparation of AChE@PILs@Au NPs

50.0 μL AChE@PILs solution was taken to a centrifuge tube, and 10.0 mL Au NPs solution was added to the tube; shake for 10 min, and observe that the solution turns from white to purple. The purple solid AChE@PILs@Au NPs composite was obtained by centrifuge separation (4000 rpm, 10 min).

Fabrication of AChE@PILs@Au NPs/GCE

The GCE was continuously polished with alumina powder, then cleaned, ultrasonically treated in a water bath, and dried with nitrogen. 10.0 μL of AChE@PILs@Au NPs solution was dripped onto the surface of the electrode. After drying at room temperature, 5.0 μL of Nafion (0.5 wt%) was dropped onto the electrode surface and completely dried at 4 ℃ to obtain the modified electrode.

Electrocatalytic and sensing performance of AChE@PILs@Au NPs/GCE

Incubate AChE@PILs@Au NPs/GCE for 10 min with standard carbaryl or DDVP solutions containing different concentrations, and then evaluate the electrochemical reaction in an electrolytic cell containing 8.0 mM ATCl in 0.1 phosphate buffer (pH 7.5). The inhibitory effect of carbaryl and DDVP is calculated as follows:

$$\text{Inhibition}(\%) = I_0 - I_1/I_0 \times 100\% \quad (1)$$

Among them, I_0 is the peak current of ATCl on the biosensor, and I_1 is the peak current of ATCl on the biosensor after carbaryl or DDVP inhibition.

Recovery studies of fruit, vegetable, and water samples

The standard addition method was used to evaluate the performance of the prepared biosensor. Tomatoes, peaches, and tap water were used in this study. First, tomatoes and peaches samples were washed with deionized water and then dried at room temperature. Then, we added 30.0 g of each sample into 150.0 mL phosphate buffer (0.1 M, pH 7.5) and mixed it well in a blender. The samples were placed in an ultrasonic bath for 5 min and then centrifuged for 10 min (4000 rpm). Subsequently, different amounts of carbaryl or DDVP were added to the fruit, vegetable, and water samples, and the electrochemical response was obtained by the differential pulse voltammetry (DPV) technique.

Results and discussion

Fabrication of AChE@PILs@Au NPs/GCE

Scheme 1 depicts the synthetic process of the as-fabricated biosensor. As shown, AChE@PILs were first synthesized using emulsion polymerization to achieve effective AChE entrapment in the form of microspheres. Because the two-component structure of AChE@PILs is positively charged overall, it may bind the negatively charged inorganic component Au NPs based on electronic static assembly. As a result, the as-prepared AChE@PILs@Au NPs behave in a three-layer core–shell structure. PILs act as a link between AChE, and Au NPs play an important role in this structure. On the one hand, PILs provide a good biocompatible microenvironment for the AChE nucleus in the inner layer, and on the other hand, it assembles the Au NPs shell in the outer layer, providing an immobilized substrate for efficient electron transport channels. The assembling of Au NPs enhances the electron transfer rate of AChE@PILs@Au NPs/GCE and amplifies the thiocholine (TCl) electrocatalytic oxidation peak current signal. When pesticides are present, the activity of AChE is inhibited and the hydrolysis process of ATCl catalyzed by AChE is inhibited, as is the electrocatalytic oxidation of the hydrolysis product TCl.

Characterization of AChE@PILs@Au NPs

The morphology of PILs, AChE@PILs, AChE@PILs@Au NPs was observed by scanning electron microscopy (SEM) (Fig. 1A, B, D). As we can see from the figures, PILs and AChE@PILs were all spherical structures formed by concentrated emulsion polymerization under the action of the template. The microemulsion of AChE@PILs contained more components than PILs. However, compared with Fig. 1A,B, the average particle size of the one-component PILs was slightly larger than the two-component AChE@PILs, which were 4.2 μm and 2.7 μm, respectively. This is because of the electrostatic interaction between AChE and PILs in the two-component system. As shown in Fig. 1C, negatively charged AChE and positively charged monomer ViEtIm^{+}Br^{-} had a strong interaction. This strong interaction

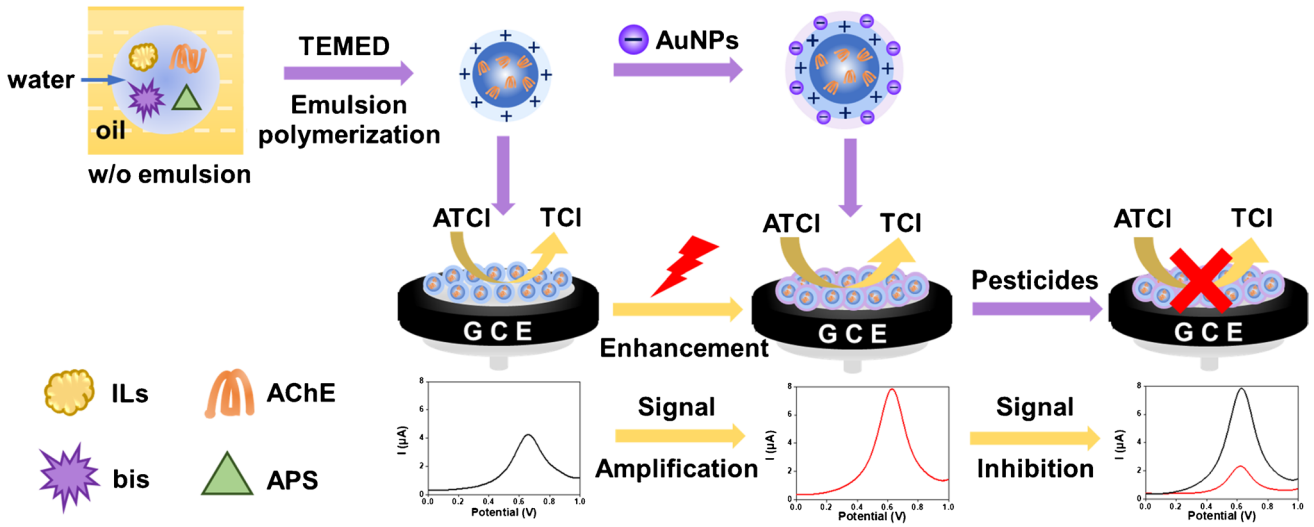

Scheme 1 Schematic illustration of the AChE biosensor structure and its working mechanism to ATCl

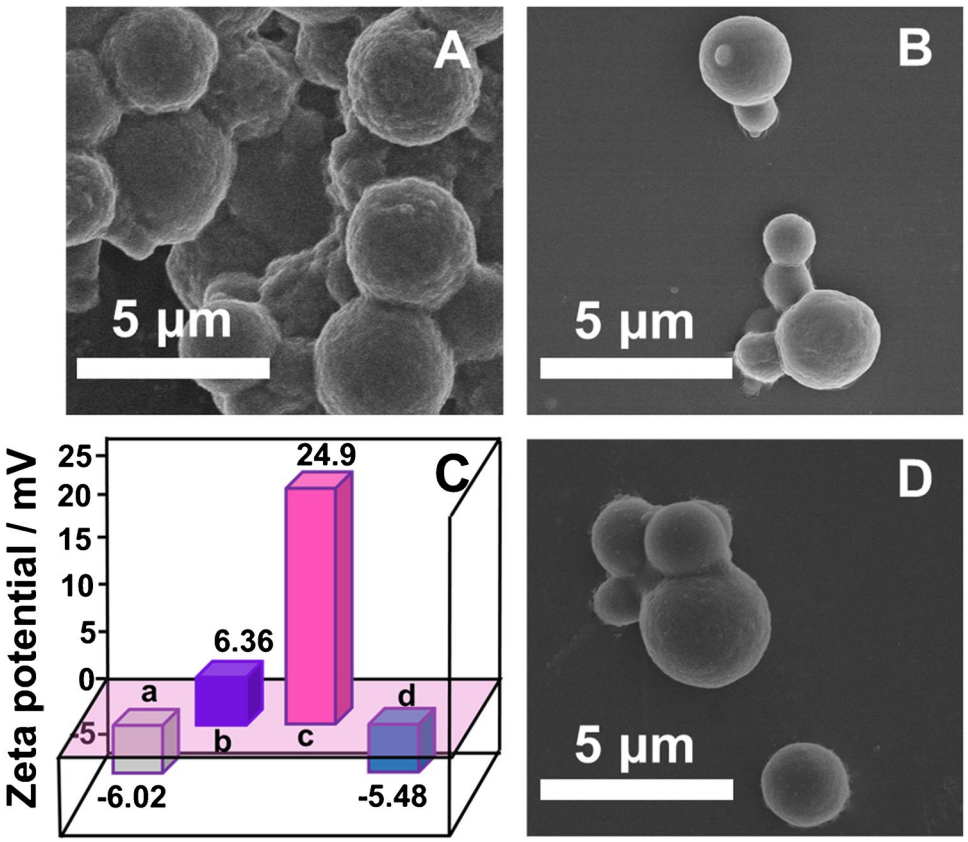

Fig. 1 SEM images of (**A**) PILs and (**B**) AChE@PILs. (**C**) zeta potential of AChE (**a**), monomer ViEtIm^{+}Br^{-} (**b**), AChE@PILs (**c**), and Au NPs (**d**). (**D**) SEM images of AChE@PILs@Au NPs

tended to form smaller polyemulsion microspheres, which led to a decrease in particle size after AChE was entrapped. As reported in a theoretical study before, when AChE is immobilized on a positively charged surface, the active site is closer to the electrode, which promotes faster electron transfer [6]. Meanwhile, zeta potentials of the binary system formed by the polymerization and Au NPs were 25 mV and − 5.5 mV, respectively (Fig. 1C), which enabled the positively charged binary system further to assemble the negatively charged Au NPs. The assembly results were shown in Fig. 1D; as can be seen, further assembly of Au NPs did not change the morphology of the binary components. Notably,

no scattered Au NPs were observed around AChE@PILs@Au NPs, indicating that Au NPs were completely loaded on the surface of AChE@PILs as an assembly. In other words, we constructed a triune composite consisting of a binary core and an Au NPs shell. The interaction between PILs and AChE was beneficial to the immobilization of the enzyme, and Au NPs could also act as a channel to achieve efficient electron transport on the electrode surface.

Figure 2A presents the FT-IR spectra of PILs, AChE@PILs, and AChE. The C = N characteristic stretching vibration peaks located in the range of 1700–1500 cm^{-1}, and the peaks located at 1440 cm^{-1} and 1160 cm^{-1} belonged to the imidazole ring which confirmed the presence of PILs. After AChE was entrapped, the peaks located at 3360 cm^{-1} and 3100 cm^{-1} appeared which were attributed to the stretching vibration of C-H in the alkyne group and benzene ring. The results were consistent with those of the AChE spectrum, which confirmed the successful entrapment of AChE. Furthermore, the π-π interaction between AChE and PILs could make them more firmly combined, which could avoid the leakage of AChE molecules.

To further investigate the chemical compositions of AChE@PILs@Au NPs, an X-ray photoelectron spectrum (XPS) was carried out. The fully scanned XPS peaks of AChE@PILs@Au NPs were shown in Fig. 2B. Elements C, N, O, and Au were detected. The high-resolution XPS spectrum of C 1 s was deconvoluted into six peaks at 286.2 eV, 285.6 eV, 285.1 eV, 284.7 eV, 284.1 eV, and 283.7 eV (Fig. 2C). The two characteristic binding energy peaks at 283.7 eV and 285.6 eV correspond to C≡C and C = N. These results also verified the existence of AChE and imidazole ring in the AChE@PILs, further confirming the successful formation of AChE@PILs. After electrostatic assembly of AChE@PILs and AuNPs, the Au 4f XPS spectrum of AChE@PILs@Au NPs displayed photoelectron lines at binding energies of 82.96 eV and 87.79 eV (Fig. 2D) [15]. This was corresponding to the peaks of Au $4f_{7/2}$ and Au $4f_{5/2}$. These results verified the existence of Au NPs in the AChE@PILs@Au NPs, further confirming the common loading between organic components, inorganic components, and enzymes in the ternary system.

The assembly of AChE@PILs and Au NPs was monitored using a UV–vis spectrum. The Au NPs solution was added to AChE@PILs and centrifuged to obtain the supernatant. The Au NPs solution itself was centrifuged under the same conditions for comparison. Supplementary Fig. S2 shows the absorption band of Au NPs (curve b), located at 519 nm. When Au NPs were combined with AChE@PILs, there was no absorption band on curve a. This could be attributed to the electrostatic assembly of positively charged AChE@PILs and negatively charged Au NPs [16]. By monitoring the assembly process, it was observed that Au NPs were effectively enriched onto the surface of the binary structure, and AChE@PILs@Au NPs ternary structure was formed.

Supplementary Fig. S3 shows the X-ray diffraction (XRD) patterns of AChE@PILs@Au NPs and AChE@PILs. The strong peaks located at 2θ = 38.184°, 44.392°, 64.576°, and 77.547° corresponded to the (111), (200), (220), and

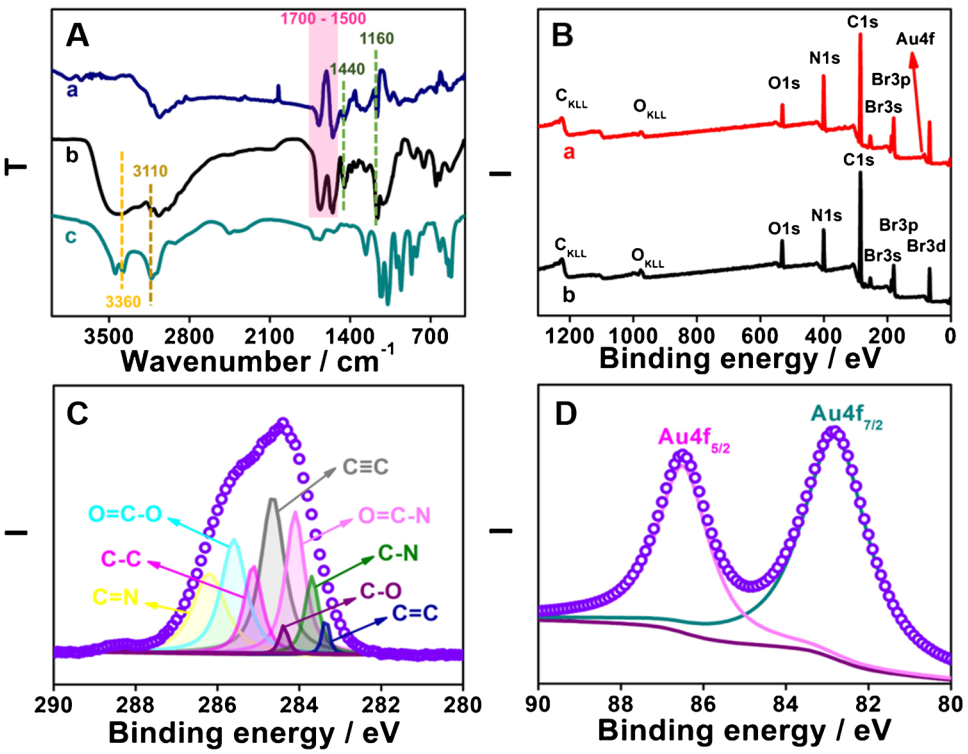

Fig. 2 (**A**) FI-IR spectrum of PILs (**a**), AChE@PILs (**b**), and AChE (**c**). (**B**) Full spectrum for AChE@PILs@Au NPs and AChE@PILs. (**C**) Au 4f and (**D**) C 1 s XPS spectrum of AChE@PILs@Au NPs

(311) diffraction patterns of typical Au [17], suggesting the successful decoration of Au NPs onto AChE@PILs.

The possible structural variation of AChE before and after entrapment can be further confirmed by the Raman spectrum (Supplementary Fig. S4). Compared with AChE@PILs@Au NPs (a) and AChE@PILs (c) in Supplementary Fig. S4A, it was obvious that the addition of Au NPs could increase the Raman signal intensity. In other words, AChE@PILs@Au NPs could achieve surface enhancement Raman spectroscopy (SERS). SERS proved that Au NPs and AChE@PILs were closely bound, and Au NPs were located on the surface of AChE@PILs instead of the environment. Supplementary Fig. S4B shows the different spectrums of the films in the presence (AChE@PILs@Au NPs) and absence (PILs@Au NPs) of AChE. The resulting spectrum closely resembled the Raman features of AChE [18], confirming the availability of enzyme active sites on the electrode surface. The region between 1620 cm^{-1} and 1700 cm^{-1} and the region between 1200 cm^{-1} and 1300 cm^{-1} were assigned to the secondary structure amine I and III from AChE [6]. The band at 1550 cm^{-1} was characteristic of tryptophan residues of the side chains, the bands from 1400 to 1500 cm^{-1} were mainly related to scissoring modes from CH_2 methylene groups, the band at 1362 cm^{-1} was due to CH_2 bending vibration, and bands between 800 cm^{-1} and 1150 cm^{-1} were considered to be the stretching vibrations from aliphatic side chains (C–C and C-N bonds) of AChE. Bands of 921 cm^{-1} and 1072 cm^{-1} were related to the presence of alanine, while the band at 946 cm^{-1} was related to lysine, glutamate, and serine. Therefore, AChE entrapped by PILs@Au NPs still had natural enzyme activity.

Electrochemical behavior of the AChE@PILs@Au NPs/GCE

The electrochemical behavior of different electrodes was examined by cyclic voltammetry (CV). Figure 3A shows the CVs for AChE@PILs@Au NPs/GCE, AChE@PILs/GCE, PILs/GCE, and GCE. All modified electrodes showed a pair of quasi reversible redox peaks with a formal potential (Ep) of 0.23 V, which is the characteristic potential of the $[Fe(CN)_6]^{3-/4-}$ electric pair. The introduction of AChE drastically decreases the currents, owing to its non-conductive property. As expected, the addition of AuNPs obviously increased the currents, indicating that Au NPs can significantly improve the conductivity of electrode materials. Figure 3B exhibits the impedance spectra of AChE@PILs@Au NPs/GCE, AChE@PILs/GCE, and PILs/GCE. Electronic transfer resistance (R_{et}) values of PILs/GCE and AChE@PILs/GCE were 28 ± 2.5 Ω and 49 ± 3.8 Ω. After AChE was entrapped, the R_{et} value increased obviously, which proved that the enzyme was immobilized successfully. It is worth noting that under the same enzyme dosage, R_{et} of the modified electrode added with Au NPs was significantly lower than AChE@PILs/GCE, which was consistent with the previous CVs analysis. Obviously, AChE@PILs@Au NPs/GCE had the lowest R_{et} value and the highest conductivity compared with AChE@PILs/GCE and PILs/GCE [19]. Figure 3C shows the results of the DPV responses of various electrodes in 0.1 M phosphate buffer containing 8.0 mM ATCl. It can be found that for three electrodes, there was no oxidation peak occurring in the lack of AChE. Oxidation peaks occurred at AChE@PILs@Au NPs/GCE and AChE@PILs/GCE. These phenomena illustrated that the entrapped AChE on PILs/GCE can catalyze the hydrolysis of ATCl to produce electroactive TCl which can be further oxidized on the surface of the electrode [20]. Comparing AChE@PILs@Au NPs/GCE and AChE@PILs/GCE, their oxidation peak currents were 6.1 ± 0.50 μA and 2.4 ± 0.34 μA, respectively. The former was 2.54 times that of the latter. The electron transfer ability of the modified electrode was significantly improved with the addition of AuNPs. The reaction process was further studied by the change of current response at different scan rates. Figure 3D shows the current response of AChE@PILs@Au NPs/GCE at different scan rates in 0.1 M, pH 7.5 phosphate buffer containing 8.0 mM ATCl. When the scan rates increased in the range of 40 to 220 mV s^{-1}, the oxidation peak current increased and the oxidation peak moves to the positive potential. As shown in the illustration, the peak current is proportional to the square root of the sweep speed, which represents the oxidation reaction on the electrode was a diffusion-controlled process.

Optimization of the biosensor

In this study, cross-linking degree, AChE concentration in the water phase, pH during the polymerization reaction, and incubation time were optimized, respectively (Supplementary Fig. S5). The following optimal parameters were selected for subsequent experiments: The degree of cross-linking was 5%, the AChE concentration in the water phase was 250 U mL^{-1}, the pH during the polymerization reaction was 8.0, and the incubation time was 10 min.

Bioelectrocatalytic activity and analytical performances

The bioelectrocatalytic activity of the optimum AChE biosensor was investigated by recording the DPV curves in a series of different concentrations of ATCl (Fig. 4A). The I value increased monotonically with the ATCl concentration changing from 0 to 10 mM. The bioelectrocatalytic response follows the Michaelis–Menten kinetics [21]. A linear $1/I$ (μA^{-1}) vs. 1/[ATCl] (mM^{-1}) plot (Fig. 4B) was obtained. By using the Lineweaver–Burk equation [Eq. (2)],

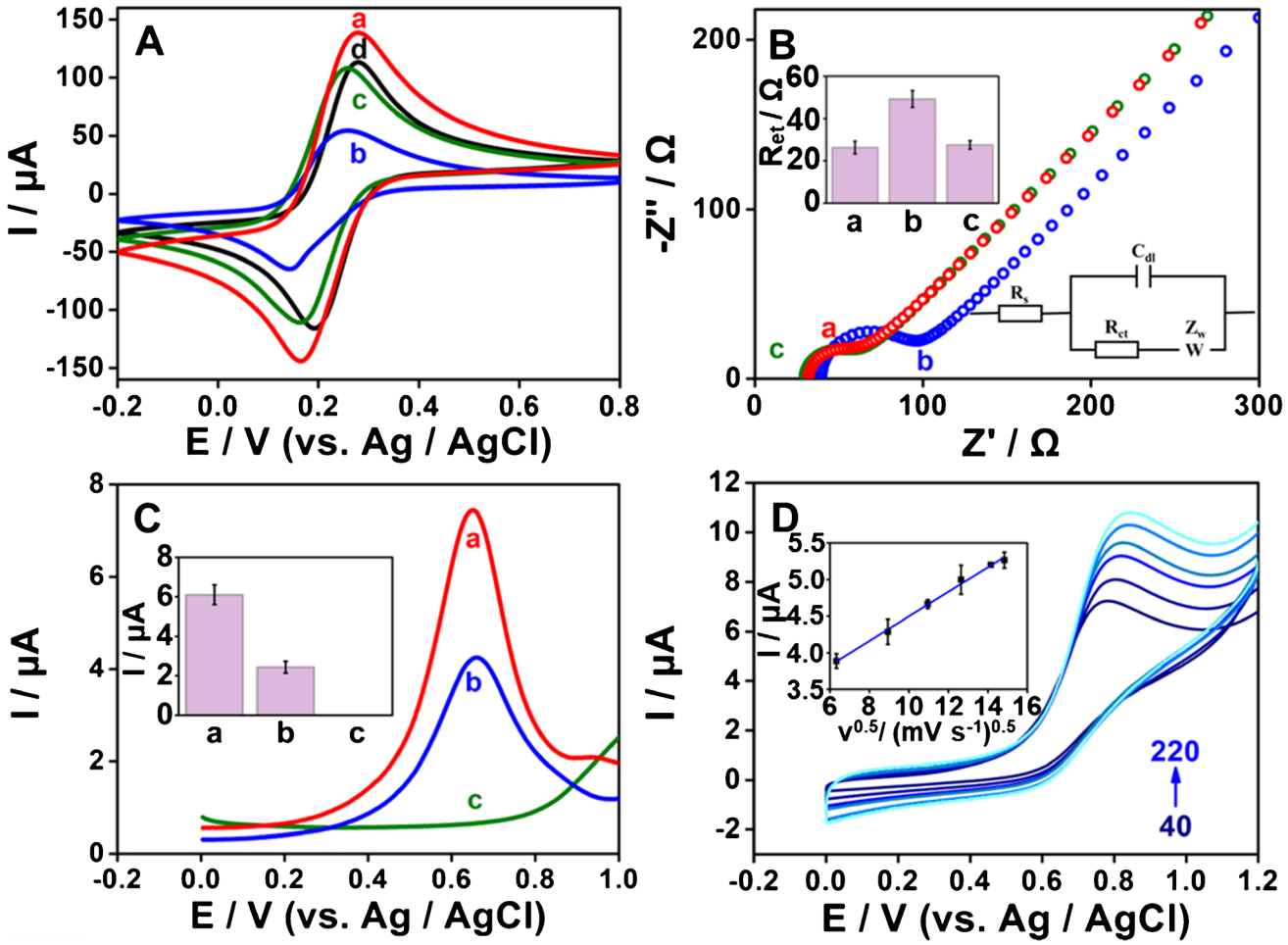

Fig. 3 (**A**) CVs for AChE@PILs@Au NPs/GCE (**a**), AChE@PILs/GCE (**b**), PILs/GCE (**c**), and GCE (**d**) in 5×10^{-3} M $Fe(CN)_6^{3-/4-}$ containing 0.1 M KCl. (**B**) EIS for AChE@PILs@Au NPs/GCE (**a**), AChE@PILs/GCE (**b**), and PILs/GCE (**c**) in 5×10^{-3} M $Fe(CN)_6^{3-/4-}$ containing 0.1 M KCl. (**C**) DPV responses of AChE@PILs@Au NPs/GCE (**a**), AChE@PILs/GCE (**b**), and PILs/GCE (**c**) in 0.1 M phosphate buffer, pH 7.5 containing 8.0 mM ATCl. (**D**) CVs for AChE@PILs@Au NPs/GCE in 0.1 M phosphate buffer, pH 7.5 containing 8.0 mM ATCl at different scan rates from 40 to 220 mV s^{-1}. Inset: a plot of peak current versus scan rate. Error bars: SD, $n=3$

the apparent Michaelis–Menten constant (K_m) was obtained to be 9.7 mM.

$$1/I = K_m/I_{\max} \cdot 1/[\text{ATCl}] + 1/I_{\max} \quad (2)$$

where I is the steady-state current after the substrate is injected. $I_{\max}$ is the maximum current calculated at saturation concentration, and [ATCl] is the substrate concentration.

The analytical performance of AChE@PILs@Au NPs/GCE exposed to a series of concentrations of two pesticides was investigated. Both carbaryl and dichlorvos have the toxicity of reducing the activity of AChE; dichlorvos inhibits AChE by the phosphorylation of the serine residue in the active site, while carbaryl carbamylate this residue [4, 8, 22]. The addition of carbaryl or DDVP could reduce the catalytic activity of AChE, and the covalent binding of the pesticide blocks the serine hydroxyl group of AChE, resulting in a reduction of the total charge of the catalytic active site, the oxidation peak current of ATCl hydrolysate decreased. The inhibition rates of the two pesticides on AChE@PILs@Au NPs/GCE were used to calculate pesticide concentrations. Under the optimized conditions described above, the analytical performance of different concentrations of carbaryl and DDVP on biosensor was tested (Fig. 4C, E). The linear relationship between inhibition measurements and pesticide concentration was obtained (Fig. 4D, F). It can be seen that the inhibition rate of carbaryl on the AChE@PILs@Au NPs/GCE-modified electrode was linear with the logarithm of its concentration. The equation was inhibition (%) = 4.8log c(carbaryl) + 14 ($R=0.98$) and inhibition (%) = 77 log c(carbaryl) − 1.4×10^2 ($R=0.99$). The linear range is observed to be 6.3×10^{-2}–1.3×10^2 ng mL^{-1} and 1.3×10^2–8.8×10^2 ng mL^{-1} with LOD of 5.1×10^{-2} ng mL^{-1} (3σ rule) and LOQ of 1.7×10^{-1} ng mL^{-1}. Similarly, the

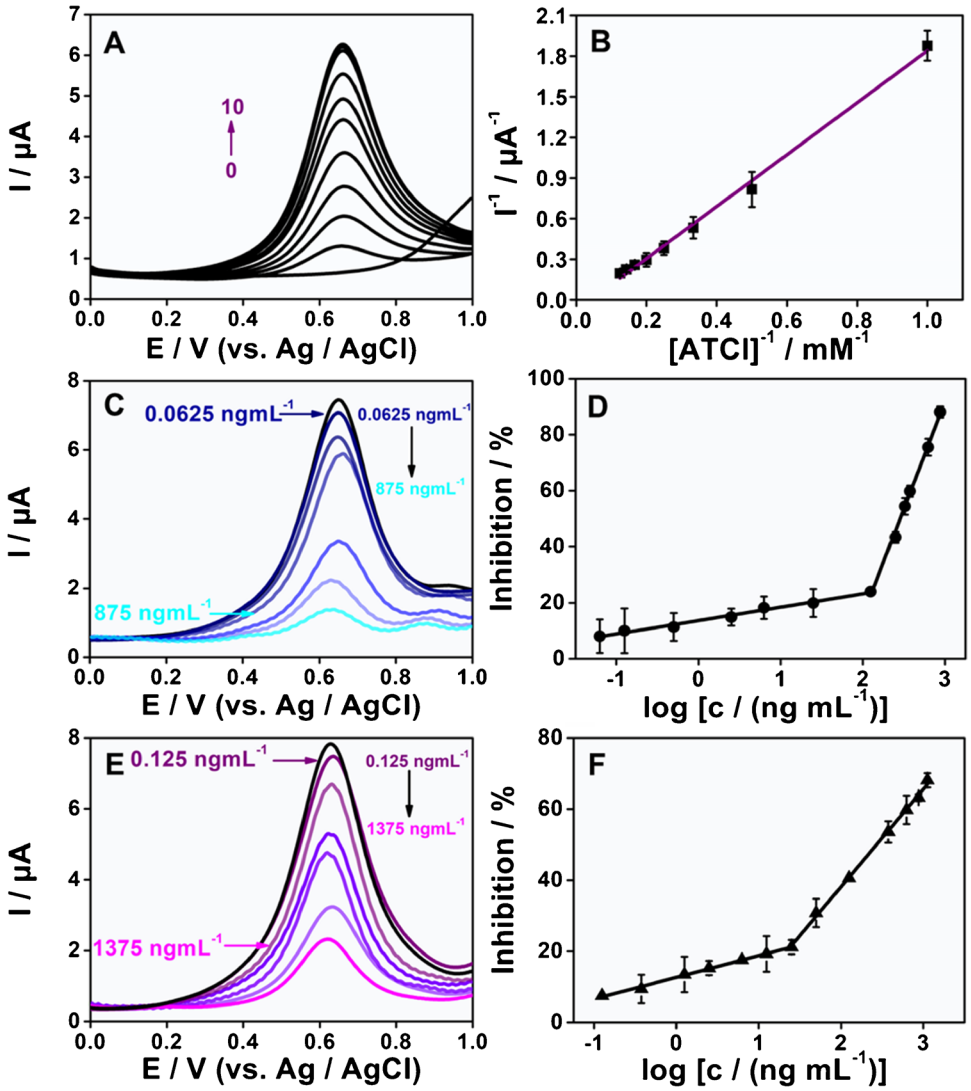

Fig. 4 (**A**) The DPV responses of the AChE@PILs@Au NPs/GCE to various concentrations of ATCl. (**B**) Plot of I^{-1} versus $[ATCl]^{-1}$. (**C**) DPV responses for AChE@PILs@Au NPs/GCE in 0.1 M phosphate buffer (pH 7.5) without and after inhibition with different concentrations of carbaryl for 10 min. (**D**) Calibration plot for carbaryl determination. (**E**) DPV responses for AChE@PILs@Au NPs/GCE in 0.1 M phosphate buffer (pH 7.5) without and after inhibition with different concentrations of DDVP for 10 min. (**F**) Calibration plot for DDVP determination. Voltage: 0.65 V, inhibition time: 10 min, error bars: SD, $n = 5$

inhibition rate of DDVP on AChE@PILs@Au NPs/GCE was linear with the logarithm of the concentration of DDVP. The equation was inhibition (%) = 6.1log c (DDVP) + 13 ($R = 0.99$) and inhibition (%) = 28log c (DDVP) − 17 ($R = 0.99$). The linear range was observed to be 1.3×10^{-1}–25 ng mL^{-1} and 25–1.4×10^{3} ng mL^{-1} with LOD of 3.9×10^{-2} ng mL^{-1} (3σ rule) and LOQ of 1.3×10^{-1} ng mL^{-1}. In addition, the results show that we classify according to the fixing method of AChE; the comparison of AChE@PILs@Au NPs/GCE with other biosensors is shown in Table 1. Compared with the biosensors that also use the entrapment method, AChE@PILs@Au NPs/GCE had the lowest LOD. Compared with other methods, except for the entrapment, AChE@PILs@Au NPs/GCE had a wider linear range and a comparable lower LOD. The wide linear range may be derived from the protection of positively charged substances against irreversible inhibition of AChE biosensors [23].

The AChE@PILs@Au NPs/GCE were stored at a temperature of 4 ℃, and the stability of the proposed biosensor was checked by repeated DPV measurements (Fig. 5A). The retained response after 30 days of storage was 95%; after 68 days, storage was 93% (Fig. 5B and Supplementary Fig. S6).

Figure 5C shows the remaining activity of the AChE@PILs@Au NPs/GCE electrodes after thermal treatment at different temperatures. It has been reported that the introduction of PILs can significantly improve the thermal stability of enzymes. Here, we use electrochemical reactions to discuss the thermal stability of the biosensor [34]. After thermal treatment of the electrodes at 35 ℃, 45 ℃, and 55 ℃ for 20 min, their remaining activity showed a trend of first increasing and then decreasing. Heated at 55 ℃ for 20 min, the entrapped AChE retained 73% of the initial activity, while the unprotected AChE was easily inactivated at high temperatures. It was previously reported that

Table 1 Comparisons of the as-prepared biosensors with other biosensors for the determination of carbaryl and DDVP

Immobilization method of AChE	Analyte	Biosensors	Storage stability	Linear range (ng mL^{-1})	Detection limit (ng mL^{-1})	References
Entrapment	Carbaryl	AChE@PILs@Au NPs/GCE	30 days (95%)	6.3×10^{-2}–8.8×10^{2}	5.0×10^{-2}	This work
		(UCNPS)/polydopamine (PDA)-based hydrogel	NR	0.50–2.0×10^{2}	0.50	[22]
		AChE/PDA-Gr/PPy NWs/IDlE	NR	50–1.5×10^{3}	8.0	[24]
	DDVP	AChE@PILs@Au NPs/GCE	30 days (95%)	1.3×10^{-1}–1.4×10^{3}	3.8×10^{-2}	This work
		Chromoionophore (ETH5294) (CM) doped sol–gel film	15 days	5.0×10^{2}–7.0×10^{3}	5.0×10^{2}	[25]
		SPE-Al_2O_3-AChE	150 days (90%)	2.2×10^{1}–1.8×10^{4}	2.2	[26]
		Au/LA/SWCNT: PEDOT/AChE	30 days (89%)	0–5.0×10^{2}	0.44	[27]
Methods except entrapment	Carbaryl	GCE/pGON-e-AChE	20 days (87%)	3.0×10^{-1}–6.1	1.5×10^{-1}	[28]
		AChE-Au NP-DS1-IC-PPy/GCE	7 days (44%)	5.0×10^{-2}–2.5×10^{-1}	3.3×10^{-2}	[6]
		G-AChE/PANI/GCE	18 days (90%)	3.8×10^{1}–1.9×10^{2}	20	[29]
		Ag/rGO/CS/AChE	NR	1.0×10^{-5}–1.0×10^{3}	1.0×10^{-9}	[30]
	DDVP	GCE/Nafion-GRO-Er-AChE	28 days (87%)	1.0–2.0×10^{1}, 5.0–10^{2}	2.0	[31]
		GCE/AChE-PB	NR	1.0×10^{-2}–10	2.5×10^{-3}	[32]
		GCE/[BSmim]HSO_4-Au NPs-porous carbon	30 days (95%)	1.0×10^{-4}–1.0	6.6×10^{-5}	[33]
		GCE/TiO_2-CS@MS@AuNRs/CS/AChE	30 days (96%)	4.0–3.0×10^{3}	1.2	[19]

Stability of the biosensor toward ATCl

unencapsulated AChE activity was reduced by 60% at 42–48 ℃ [35]. Obviously, the thermal stability of AChE is significantly improved due to its entrapment; the PILs layer can minimize the impact of the microenvironment changes on AChE. This performance can be used to dissolve pesticides in actual samples at high temperatures and can be directly detected in hot solutions without cooling, which improves efficiency.

Repeatability and anti-interference studies of the biosensor toward ATCl

In addition, the repeatability was studied by using DPV to perform 5 measurements under constant conditions, with an RSD value of only 3.68%. The anti-interference studies were evaluated by measuring the amperometric response in the presence of some possible interferents, such as glucose, PO_4^{3-}, citric acid, metal ions, inorganic salts, and pesticides. The results were shown in Fig. 5D. In the presence of glucose, citric acid, Mg^{2+}, SO_4^{2-}, NO_3^{-}, Fe^{3+}, and Cu^{2+}, almost no significant interference was observed. In addition, the addition of chlorpyrifos and malathion was also studied. AChE@PILs@Au NPs/GCE responded to all three pesticides. The results showed that the constructed biosensor responded to both organophosphorus and carbamates pesticides.

To confirm the sensitivity and applicability of the method, tomatoes and peaches were tested by modified electrodes (Supplementary Table S1). Recovery studies were carried out in fruit, vegetable, and water samples by the standard addition method. The recoveries ranged from 96.9 to 102.6%. These results showed that the proposed biosensor is feasible in practical applications.

Conclusions

A highly stable electrochemical biosensor for pesticide detection was successfully developed. The AChE@PILs@Au NPs/GCE electrochemical biosensor was constructed by entrapping AChE in PILs with subsequent immobilization of negatively charged Au NPs through the electrostatic assembly. The result showed that positively charged PILs not only provide a biocompatible microenvironment around the AChE molecule to maintain activity and prevent its leakage but also improve the stability of the immobilized AChE molecule. The introduction of PILs also realized the combination of Au NPs to improve the electrical conductivity of the electrode material. The detection of carbaryl and DDVP

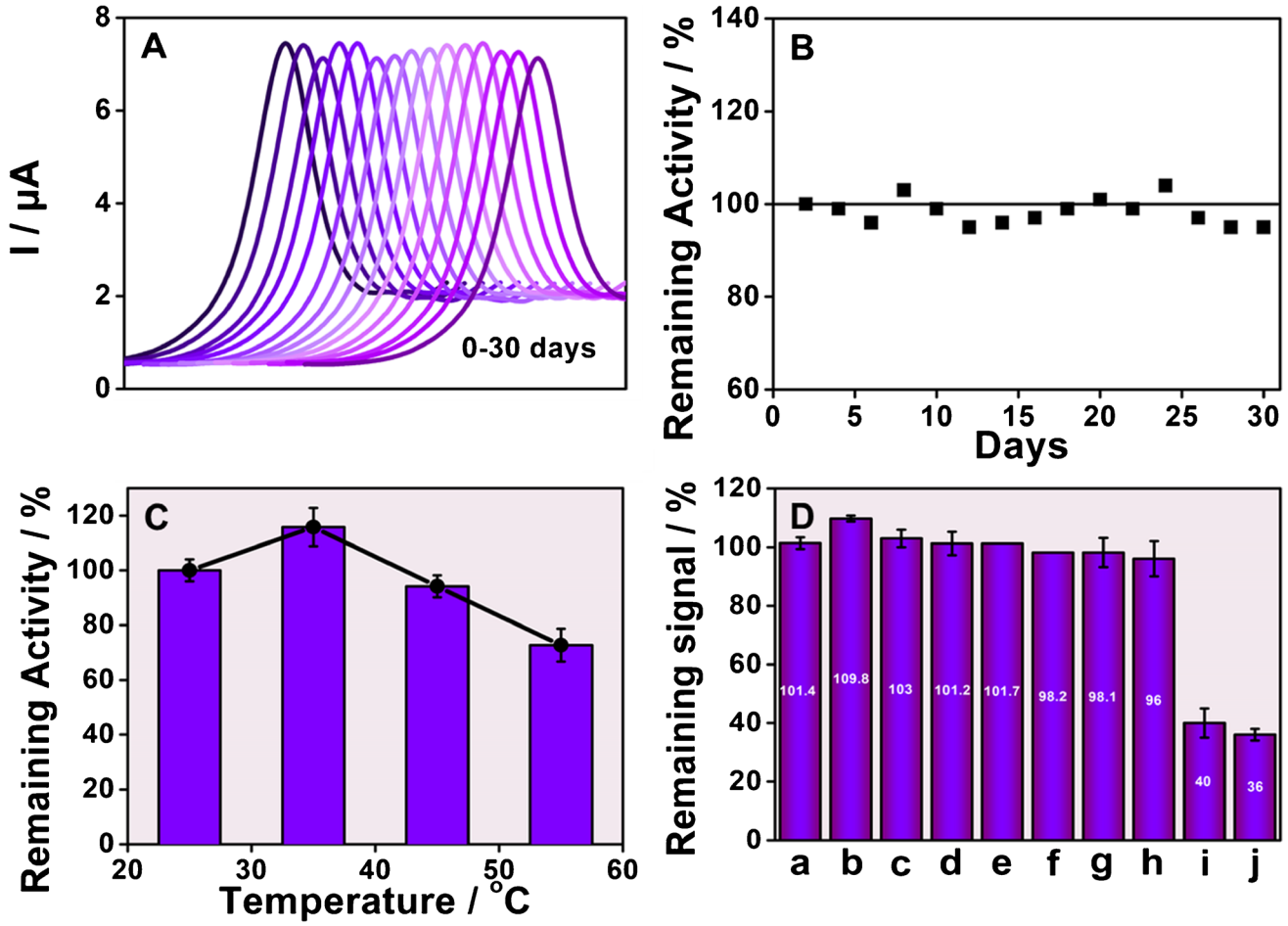

Fig. 5 (**A**) DPV responses of AChE@PILs@Au NPs/GCE in 0.1 M phosphate buffer (pH 7.5) in the presence of 8.0 mM ATCl during 30 days. (**B**) The stability of the biosensor response measured during 30 days. (**C**) Effect of the temperature on the activity of an AChE@PILs@Au NPs/GCE in 0.1 M phosphate buffer (pH 7.5) in the presence of 8.0 mM ATCl. (**D**) Remaining signal in 0.1 M phosphate buffer containing 8.0 mM ATCl in the presence of 8.0 mM of glucose (**a**), 8.0 mM of PO_4^{3-} (**b**), 8.0 mM of citric acid (**c**), 8.0 mM of Mg^{2+} (**d**), 8.0 mM of SO_4^{2-} (**e**), 8.0 mM of NO_3^- (**f**), 8.0 mM of Fe^{3+} (**g**), 8.0 mM of Cu^{2+} (**h**), 200 ng mL^{-1} chlorpyrifos (**i**), and 200 ng $mL^{-.1}$ malathion (**j**) after being incubated for 10 min. Error bars: SD, $n = 3$

by such a biosensor has a super-wide linear range and a low detection limit. In addition, the biosensor constructed has good repeatability, anti-interference ability, high thermal stability and storage stability, and has high accuracy in the analysis of peaches, tap water, and other practical samples. Moreover, the improvement of the thermal stability of the immobilized enzyme was realized. The π-π conjugation effect of PILs gives it the potential to combine with other carbon-based components, which expands the application prospect of materials.

Supporting information

Size distribution of PILs and AChE@PILs in water; UV–vis spectrum for supernatant of AChE@PILs@Au NPs and Au NPs; XRD patterns for AChE@PILs@Au NPs and AChE@PILs; Raman spectrum of AChE@PILs@Au NPs, PILs@Au NPs and AChE@PILs; Difference Raman spectrum between PILs@Au NPs and AChE@PILs@Au NPs; Effect of the cross-linking ratio, AChE concentration, pH during polymerization, incubation time; Stability study of AChE@PILs@Au NPs/GCE during 68 days; Recovery studies of spiked carbaryl and DDVP in fruit, vegetable and water samples.

Supplementary Information The online version contains supplementary material available at https://doi.org/10.1007/s00604-022-05383-6.

Acknowledgements Authors Yu Wan, Huiting Wang Yaxian Chen, Shun Li, Jie Zhou, and Lixin Xia* received funding from the National Natural Science Foundation of China (21671089), the Liaoning Revitalization Talents Program (XLYC2002097), the Scientific Research Fund of Liaoning Provincial Education Department (L2020002), and the Liaoning Provincial Natural Science Foundation (2020-YKLH-22). Authors Yu Wan, Huiting Wang, Ling Zhang, Yaxian Chen, Shun Li, Jie Zhou, and Qian Zhang* received funding from the

Scientific Research Fund of Liaoning Provincial Education Department (LR2019029).

Author contribution The manuscript was written through the contributions of all authors. All authors have given approval to the final version of the manuscript.

Declarations

Competing interests The authors declare no competing interests.

References

1. Sharma P, Pandey V, Sharma MMM et al (2021) A review on biosensors and nanosensors application in agroecosystems. Nanoscale Res Lett 16:136. https://doi.org/10.1186/s11671-021-03593-0
2. Khanmohammadi A, Jalili Ghazizadeh A, Hashemi P et al (2020) An overview to electrochemical biosensors and sensors for the detection of environmental contaminants. J Iran Chem Soc 17:2429–2447. https://doi.org/10.1007/s13738-020-01940-z
3. Pajooheshpour N, Rezaei M, Hajian A et al (2018) Protein templated Au-Pt nanoclusters-graphene nanoribbons as a high performance sensing layer for the electrochemical determination of diazinon. Sensor Actuat B-Chem 275:180–189. https://doi.org/10.1016/j.snb.2018.08.014
4. Pundir CS, Malik A, Preety, (2019) Bio-sensing of organophosphorus pesticides: a review. Biosens Bioelectron 140:111348. https://doi.org/10.1016/j.bios.2019.111348
5. Zhao HY, Ma HN, Li XG et al (2021) Nanocomposite of halloysite nanotubes/multi-walled carbon nanotubes for methyl parathion electrochemical sensor application. Appl Clay Sci 200:105907. https://doi.org/10.1016/j.clay.2020.105907
6. Loguercio LF, Thesing A, Demingos P et al (2021) Efficient AChE immobilization for improved electrochemical performance in polypyrrole nanocomposite-based biosensors for carbaryl pesticide. Sens Actuators B Chem 339:129875. https://doi.org/10.1016/j.snb.2021.129875
7. Liu XF, Wu ZX, Yang XH et al (2020) Photothermal and fluorescent dual-mode assay based on the formation of polydopamine nanoparticles for accurate determination of organophosphate pesticides. Microchim Acta 187:652. https://doi.org/10.1007/s00604-020-04629-5
8. Cao J, Wang M, Yu H et al (2020) An overview on the mechanisms and applications of enzyme inhibition-based methods for determination of organophosphate and carbamate pesticides. J Agric Food Chem 68:7298–7315. https://doi.org/10.1021/acs.jafc.0c01962
9. Lee CH, Jin ES, Lee JH et al (2020) Immobilization and stabilization of enzyme in biomineralized calcium carbonate microspheres. Front Bioeng Biotech 8:553591. https://doi.org/10.3389/fbioe.2020.553591
10. López Sánchez-Paniagua M, Mecerreyes D, López-Cabarcos E, López-Ruiz B (2006) Amperometric glucose biosensor based on polymerized ionic liquid microparticles. Biosens Bioelectron 21:2320–2328. https://doi.org/10.1016/j.bios.2006.02.019
11. Radulescu MC, Bucur MP, Bucur B et al (2019) Ester flavorants detection in foods with a bienzymatic biosensor based on a stable Prussian blue-copper electrodeposited on carbon paper electrode. Talanta 199:541–546. https://doi.org/10.1016/j.talanta.2019.02.094
12. Bagheri H, Ranjbari E, Amiri-Aref M et al (2016) Modified fractal iron oxide magnetic nanostructure: a novel and high performance platform for redox protein immobilization, direct electrochemistry and bioelectrocatalysis application. Biosens Bioelectron 85:814–821. https://doi.org/10.1016/j.bios.2016.05.097
13. Gao SS, Liu J, Luo J et al (2018) Selective voltammetric determination of Cd(II) by using N, S-codoped porous carbon nanofibers. Microchim Acta 185:1–9. https://doi.org/10.1007/s00604-018-2818-2
14. Lebedeva O, Kultin D, Kustov L (2021) Electrochemical synthesis of unique nanomaterials in ionic liquids. Nanomaterials 11:3270. https://doi.org/10.3390/nano11123270
15. Karpenko A, Leppelt R, Cai J et al (2007) Deactivation of a Au/CeO_2 catalyst during the low-temperature water-gas shift reaction and its reactivation: a combined TEM, XRD, XPS, DRIFTS, and activity study. J Catal 250:139–150. https://doi.org/10.1016/j.jcat.2007.05.016
16. Singh S, Tripathi P, Kumar N et al (2016) Colorimetric sensing of malathion using palladium-gold bimetallic nanozyme. Biosens Bioelectron 92:280–286. https://doi.org/10.1016/j.bios.2016.11.011
17. Uosaki K, Shen Y, Kondo T (1995) Preparation of a highly ordered Au (111) phase on a polycrystalline gold substrate by vacuum deposition and its characterization by XRD, GISXRD, STM/AFM, and electrochemical measurements. J Phys Chem 99:14117–14122. https://doi.org/10.1021/j100038a051
18. Aslanian D, Grof P, Bon S et al (1991) A comparative Raman spectroscopic study of cholinesterases. Biochimie 73:1375–1386. https://doi.org/10.1016/0300-9084(91)90167-Y
19. Cui HF, Wu WW, Li MM et al (2018) A highly stable AChE biosensor based on chitosan-TiO_2-graphene nanocomposites for detection of organophosphate pesticides. Biosens Bioelectron 99:223–229. https://doi.org/10.1016/j.bios.2017.07.068
20. Cui HF, Zhang TT, Lv QY et al (2019) An AChE biosensor based on doping Au nanorod@SiO_2 nanoparticles into TiO_2-chitosan hydrogel for detection of organophosphate pesticides. Biosens Bioelectron 141:111452. https://doi.org/10.1016/j.bios.2019.111452
21. Mahmoudi E, Fakhri H, Hajian A et al (2019) High-performance electrochemical enzyme sensor for organophosphate pesticide detection using modified metal-organic framework sensing platforms. Bioelectrochemistry 130:107348. https://doi.org/10.1016/j.bioelechem.2019.107348
22. Su DD, Zhao X, Yan X et al (2021) Background-free sensing platform for on-site detection of carbamate pesticide through upconversion nanoparticles-based hydrogel suit. Biosens Bioelectron 194:113598. https://doi.org/10.1016/j.bios.2021.113598
23. Shamagsumova RV, Shurpik DN, Padnya PL et al (2015) Acetylcholinesterase biosensor for inhibitor measurements based on glassy carbon electrode modified with carbon black and pillar[5]arene. Talanta 144:559–568. https://doi.org/10.1016/j.talanta.2015.07.008
24. Ha TB, Le HT, Cao HH (2018) Electro-immobilization of acetylcholinesterase using polydopamine for carbaryl microsensor. J Electron Mater 47:1686–1693. https://doi.org/10.1007/s11664-017-5880-3
25. Wong FCM, Ahmad M, Heng LY et al (2006) An optical biosensor for dichlovos using stacked sol-gel films containing acetylcholinesterase and a lipophilic chromoionophore. Talanta 69:888–893. https://doi.org/10.1016/j.talanta.2005.11.034
26. Shi MH, Xu JJ, Zhang S et al (2006) A mediator-free screen-printed amperometric biosensor for screening of organophosphorus pesticides with flow-injection analysis (FIA) system. Talanta 68:1089–1095. https://doi.org/10.1016/j.talanta.2005.07.007
27. Tutunaru O, Mihailescu CM, Savin M et al (2016) Acetylcholinesterase entrapment onto carboxyl-modified single-walled carbon nanotubes and poly (3,4-ethylenedioxythiophene) nanocomposite, film electrosynthesis characterization, and sensor

application for dichlorvos detection in apple juice. Microchem J 169:106573. https://doi.org/10.1016/j.microc.2021.106573
28. Li YP, Zhao RX, Shi LY et al (2017) Acetylcholinesterase biosensor based on electrochemically inducing 3D graphene oxide network/multi-walled carbon nanotube composites for detection of pesticides. RSC Adv 7:53570–53577. https://doi.org/10.1039/c7ra08226f
29. Li YP, Shi LY, Han GY et al (2017) Electrochemical biosensing of carbaryl based on acetylcholinesterase immobilized onto electrochemically inducing porous graphene oxide network. Sens Actuators B Chem 238:945–953. https://doi.org/10.1016/j.snb.2016.07.152
30. Mashuni M, Ritonga H, Jahiding M et al (2022) Highly sensitive detection of carbaryl pesticides using potentiometric biosensor with nanocomposite Ag/r-graphene oxide/chitosan immobilized acetylcholinesterase enzyme. Chemosensors 10:138. https://doi.org/10.3390/chemosensors10040138
31. Wu S, Huang FF, Lan XQ et al (2012) Electrochemically reduced graphene oxide and Nafion nanocomposite for ultralow potential detection of organophosphate pesticide. Sens Actuators B Chem 177:724–729. https://doi.org/10.1016/j.snb.2012.11.069
32. Sun X, Wang XY (2010) Acetylcholinesterase biosensor based on Prussian blue-modified electrode for detecting organophosphorous pesticides. Biosens Bioelectron 25:2611–2614. https://doi.org/10.1016/j.bios.2010.04.028
33. Wei M, Wang JJ (2015) A novel acetylcholinesterase biosensor based on ionic liquids-Au NPs-porous carbon composite matrix for detection of organophosphate pesticides. Sens Actuators B Chem 211:290–296. https://doi.org/10.1016/j.snb.2015.01.112
34. Liu Y, Wang MJ, Li J et al (2005) Highly active horseradish peroxidase immobilized in 1-butyl-3-methylimidazolium tetrafluoroborate room-temperature ionic liquid based sol-gel host materials. Chem Commun 1778–1780.
35. Edwards JA, Brimijoin S (1983) Thermal inactivation of the molecular forms of acetylcholinesterase and butyrylcholinesterase. Biochim Biophys Acta 742:509–516. https://doi.org/10.1016/0167-4838(83)90268-6